Universal characteristics of resonant–tunneling field emission from nanostructured surfaces

S. Johnson,[1] U. Zülicke,[2,3] and A. Markwitz[1,3]

[1]*Institute of Geological and Nuclear Sciences, PO Box 31-312, 30 Gracefield Road, Lower Hutt, New Zealand*
[2]*Institute of Fundamental Sciences, Massey University, Private Bag 11 222, Palmerston North, New Zealand*
[3]*MacDiarmid Institute for Advanced Materials and Nanotechnology, PO Box 600, Wellington, New Zealand*

(Dated: February 1, 2008)

We have performed theoretical and experimental studies of field emission from nanostructured semiconductor cathodes. Resonant tunneling through electric–field–induced interface bound states is found to strongly affect the field–emission characteristics. Our analytical theory predicts power–law and Lorentzian–shaped current–voltage curves for resonant–tunneling field emission from three–dimensional substrates and two–dimensional accumulation layers, respectively. These predicted line shapes are observed in field emission characteristics from self–assembled silicon nanostructures. A simple model describes formation of an accumulation layer and of the resonant level in these systems.

I. INTRODUCTION

Field emission describes the ejection of electrons from a conducting substrate into vacuum via electron tunneling through the surface potential barrier.[1,2] As tunneling is a sensitive probe of the electronic spectrum, field emission has often been applied as a useful spectroscopic tool for bulk–material characterization.[3] Experiments using *nanostructured* emitters[4,5] reveal deviations from conventional theory,[1,2] signifying that, in these systems, tunneling occurs through discrete energy levels formed in the nanotips due to spatial confinement. In addition to revealing intriguing properties of electron transport at the nanoscale, the intense and highly coherent electron beams extracted from such nanotips have found useful applications in projection electron holography.[6] More recently, a number of field–emission studies of 2D (quantum film), 1D (quantum wire),[7,8] and 0D (quantum dot)[9] *semiconductor* systems have also demonstrated clear deviations from Fowler–Nordheim behavior. In particular, discrete current peaks, an anomalously low threshold field for electron emission and regions of negative differential conductance have all been observed in the current–voltage (*I*–*V*) field–emission characteristics. All of these features are associated with the formation of quantized bound states in the low–dimensional semiconductor cathodes. These experimental results have stimulated a number of theoretical studies of electron field emission from and through quantum–confined electronic states.[10,11,12,13,14]

In this work, we consider a generic system consisting of a bulk semiconductor substrate (S) with a nanostructured surface where nanometer–sized tips ('whiskers') have formed. In addition to the energy barrier between electronic states in the nanostructure (N) and vacuum (V), quantum confinement gives rise to a further barrier at the substrate–nanostructure (S–N) interface. Electric–field penetration into the semiconductor material leads to band bending[15,16] and the formation of 2D bound states at both interfaces. The evolution of bound–state formation is illustrated in Fig. 1 for a set of model parameters. We focus on the situation shown where, initially, a 2D bound state is formed at the S–N interface. See Fig. 1(a). As its energy lies below the substrate conduction–band edge, no resonant tunneling can occur via this state. As the electric field is increased further, quantization of electron energy also occurs within the potential well formed at the N–V interface, as shown in Fig. 1(b). The corresponding bound states can mediate resonant tunnelling both from the 3D substrate electron system and also from the 2D bound states formed in the S–N quantum well. Here we present results from our analytical theory which describes resonant–tunneling field emission from such 3D and 2D systems. These studies provide new insight into universal features exhibited in field emission from nanostructured surfaces and which are confirmed by our measurements of field–emission currents from self–assembled silicon nanostructures. In particular, resonant tunneling from a 3D substrate via a 2D interface bound state is found to give rise to a power law $I \propto V^{5/3}$ in the ascending part of the resonance peak in the *I*–*V* curve. The clear contrast to Fowler–Nordheim theory, which predicts $I \propto V^2$, allows for unambiguous identification of the 3D–vacuum resonant–tunneling mechanism. Alternatively, when resonant tunneling through the 2D interface bound state occurs from a 2D accumulation layer, the peak exhibits a Lorentzian line shape. We start by describing the theoretical method and results. This is followed

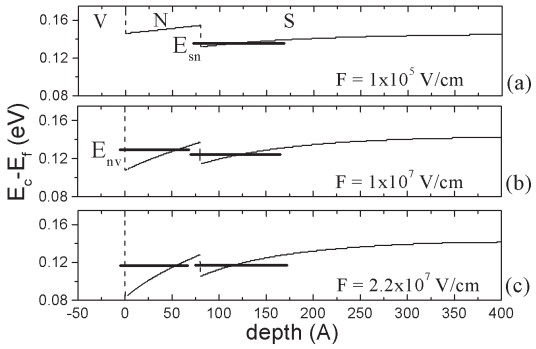

FIG. 1: Energy band diagram of a realistic model for a vacuum–nanostructure–substrate system based on a silicon nanostructure 8 nm high and 10 nm in diameter. The external electric field F is increasing in successive panels (a)–(c). V, N, and S correspond to the vacuum, nanostructure and substrate regions, while $E_{\rm sn}$ and $E_{\rm nv}$ correspond to the lowest energy bound states located at the substrate–nanostructure and nanostructure–vacuum interfaces respectively.

by details of our sample preparation, measurement setup, and the obtained field–emission data.

II. THEORETICAL ANALYSIS

The general expression for the field–emission current density from a cathode as a function of temperature T and voltage V is given by[13,17]

$$j_{\rm FE}(T,V) = \frac{e}{\pi\hbar}\int_0^\infty dE\ \ T(E,V)\,N(E,T,V) \quad . \qquad (1)$$

Here $T(E,V)$ denotes the energy–dependent quantum–mechanical transmission function from electrode to vacuum, and $N(E,T,V)$ is the supply function of the electron reservoir, i.e., the density of electrons in transverse plane–wave states having energy E in their motion perpendicular to the interfaces. The substrate-vacuum voltage drop V is proportional to the applied electric field F, with the constant of proportionality being dependent on the specific experimental geometry and system under consideration. We proceed now to discuss the form of the transmission and supply functions employed in our transport calculations before stating the results of our analytical theory.

Resonant tunneling through a 2D bound state, e.g., the one formed at the N–V interface shown in Fig. 1, can be described phenomenologically[17] by a Lorentzian energy dependence of the transmission coefficient,

$$T_{\rm RT}(E) = T_{\rm pk}\left[1+4\left(\frac{E-E_{\rm nv}}{\Gamma_{\rm nv}}\right)^2\right]^{-1} \quad , \qquad (2)$$

where $E_{\rm nv}$ and $\Gamma_{\rm nv}$ are the resonance energy and life–time broadening, respectively, of the bound state at the N–V interface. $T_{\rm pk}$ is the transmission probability at resonance. As the double–barrier system under consideration is highly asymmetric, with a high (low) barrier at the N–V (S–N) interface, the peak transmission is dominated by Fowler–Nordheim tunneling[18] through the N–V barrier. The relation

$$\frac{\pi}{2}\,T_{\rm pk}\,\Gamma_{\rm nv} \approx E_{\rm nv}\,T_{\rm nv}(E_{\rm nv}) \qquad (3)$$

can then be derived,[17] with the transmission function for tunneling through the N–V barrier denoted by $T_{\rm nv}(E)$.

The explicit form of the supply function depends on the dimensionality of the electron reservoir. For field emission from a 3D substrate, it is given by the familiar expression[17]

$$N_{\rm sub}(E,T,V) = \frac{mk_{\rm B}T}{2\pi\hbar^2}\,\ln\left(1+e^{\frac{\mu_{\rm s}+eV-E}{k_{\rm B}T}}\right) \quad , \qquad (4)$$

with $k_{\rm B}$ denoting the Boltzmann constant, m being the effective mass of electrons in the substrate, and $\mu_{\rm s}$ the equilibrium chemical potential of the substrate. The supply function is modified, however, when a 2D system such as the accumulation layer formed at the S–N interface acts as the electron reservoir. While the energy of electron motion transverse to interfaces is quantized in a quantum well, coupling of the bound state to substrate and nanostructure lead to a finite life time of electrons in the accumulation layer. Hence it supplies electrons with energies in a narrow range $\Gamma_{\rm sn}$ around the bound–state energy $E_{\rm sn}$ with a Lorentzian distribution,[13] yielding

$$N_{\rm acc}(E,T,V) = N_{\rm sub}(E,T,V)\left[1+4\left(\frac{E-E_{\rm sn}}{\Gamma_{\rm sn}}\right)^2\right]^{-1} . \qquad (5)$$

Having specified transmission and supply functions, we are in the position to calculate the field–emission characteristics using Eq. (1). To obtain our analytical results, we make the following assumptions: (i) presence of a highly degenerate electron gas in the reservoir, which means that we use the $T \to 0$ limiting expression for the supply functions, and (ii) triangular shape of the N–V quantum well, which allows us to express $E_{\rm nv}$ in terms of the applied electric field F as[17] $E_{\rm nv} = (\hbar^2\pi^2/2m\varepsilon^2)^{1/3}(eF)^{2/3}$. We find then the following expressions for the *I–V* characteristics of resonant–tunneling field emission from a 3D substrate and from a 2D accumulation layer, respectively:

$$j^{\rm (3D)}_{\rm RTFE}(V) = \frac{e^2m}{2\pi^2\hbar^3}\left(\frac{\pi^2\hbar^2}{2m\kappa D^2}\right)^{\frac{1}{3}}(eV)^{\frac{5}{3}}\exp\left[-\frac{V_0}{V}\right]\,\theta\left(\mu_{\rm s}-E_{\rm nv}\right)\theta\left(E_{\rm nv}-E_{\rm bs}\right) \quad , \qquad (6a)$$

$$j^{\rm (2D)}_{\rm RTFE}(V) = j^{\rm (3D)}_{\rm RTFE}(V)\ \frac{\Gamma_{\rm sn}}{\Gamma_{\rm sn}+\Gamma_{\rm nv}}\ \frac{\theta\left(\mu_{\rm s}-E_{\rm sn}\right)}{1+\left[2\frac{E_{\rm sn}-E_{\rm nv}}{\Gamma_{\rm sn}+\Gamma_{\rm nv}}\right]^2} \quad . \qquad (6b)$$

Here κ denotes the dielectric constant of the substrate material, D is the distance over which the cathode potential is dropped, and V_0 is a voltage scale related to the effective work function of the vacuum barrier, which is modified due to energy quantisation. The Heaviside step functions $\theta(x)$ in Eqs. (6) enforce proper phase–space conditions for resonant–tunneling transport to occur, e.g., cutting the current off sharply when the (in general voltage–dependent) resonant–level energy $E_{\rm nv}$ falls below the conduction–band bottom $E_{\rm bs}$. The conspicuous difference in the voltage–

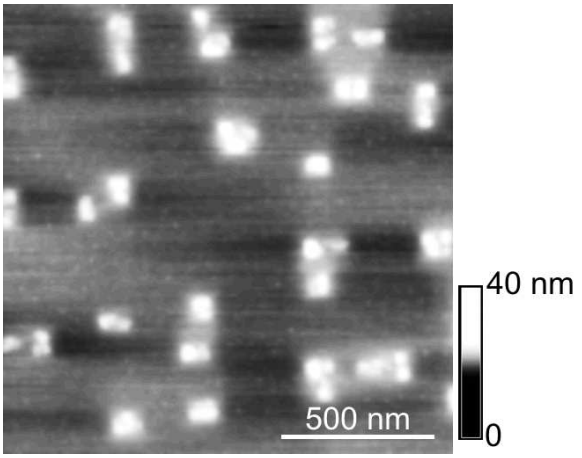

FIG. 2: 1.5 μm$\times$1.5μm AFM surface plot of the Si nanostructures formed by electron beam annealing at 1000 °C for 15 s. The rate at which the sample was heated and cooled was 5 °C/s.

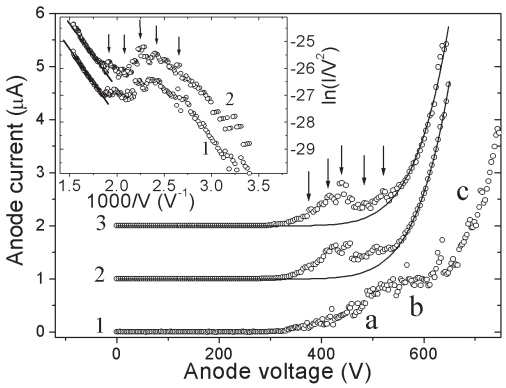

FIG. 3: *I–V* field emission characteristics for Si nanostructures formed on n-type Si (100) substrate. The three curves correspond to successive conditioning cycles, where 1 corresponds to the first and 3 the final conditioning cycle . The solid lines that overlay curves 2 and 3 correspond to a fit to Fowler–Nordheim theory. For clarity, each curve has been offset by 1 μA . The inset shows Fowler-Nordheim plots of curves 1 and 2. The arrows indicate the positions of the five most prominent peaks, while the solid lines indicate the best fit for the experimental data in the Fowler–Nordheim emission region. Curve 2 has been offset by 1 along the y-axis.

dependent pre-exponential factor of Eq. (6a) compared to the Fowler–Nordheim formula [$(eV)^{5/3}$ as opposed to $(eV)^2$] arises from the field dependence of the bound–state energy $E_{\rm nv} \propto (V/D)^{2/3}$ formed in the triangular N–V quantum well.

III. EXPERIMENTAL PROCEDURE

We now proceed to describe details of our experimental study which examines the field–emission properties of a self–assembled silicon nanostructure formed on a silicon substrate.[19] Detailed analysis of the *I–V* field–emission characteristics indicates the presence of two classes of current peaks which occur at different regions of electric field. Based on our understanding gained from theoretical analysis described above, we can relate these two classes of current peaks to resonant tunnelling from the 3D substrate and from 2D bound states located at the N–S interface, respectively. In both cases, tunnelling is mediated by a second set of 2D bound states located at the N–V interface.

Substrates used in the present study were n-type Si (100) wafers (P-doped, conductance 1–10 Ωcm , corresponding to a dopant density of 10^{15}–10^{16} cm^{-3}). Nanostructure growth results from annealing of the untreated substrates to 1000 °C for 15 s using a 20 keV raster–scanned electron beam. Details of the fabrication procedure and mechanism for nanostructure growth have been reported elsewhere.[20] A characteristic AFM image of the nanostructured Si substrate surface is shown in Fig. 2. The self-assembled nanostructures are square–based and distributed randomly over the surface with a density of 11 μm^{-2}. High–resolution AFM and TEM studies[21] indicate an average nanostructure height of 8 nm and a base length distribution in the range 8–60 nm. The relevance of these structures to the study of 3D and 2D resonant–tunnelling field emission phenomena of the type discussed theoretically above, becomes apparent when one considers an energy band diagram of the S–N–V system. In the first case, the S–N interface was modelled by an offset in the conduction band equal to the confinement energy of the lowest–lying transverse bound state in the nanostructure. Self-consistent solutions of the Poisson and Schrödinger equations were then used to calculate the conduction–band–bottom profile and to find regions of electron energy quantization.[22] Given the size distribution of the nanostructures, and assuming a rectangular quantum well, the offset in the conduction band was calculated to be in the range 0.6–31 meV with bound states located at the S–N interface forming only in those structures smaller than 12 nm. Fig. 1 shows the results of our simulations for a 10 nm diameter silicon nanostructure.

IV. RESULTS AND DISCUSSION

Characterisation of the field–emission properties of these self-assembled nanostructures was performed at room temperature in a parallel–plate diode configuration. Electrical isolation and cathode–anode separation was achieved using a 100 μm thick PTFE film, and measurements were performed under vacuum of 1×10^{-7}mbar. It was found necessary to run several emission cycles at high emission currents (5 μA) in order for the *I–V* characteristics to become stable and reproducible. The measured anode voltage can be related to the voltage drop V, defined in the equations above, via a lever-arm relationship. The *I–V* curves plotted in Fig. 3 show the change in emission current during the course of a conditioning cycle. The nanostructured substrate was maintained under vacuum between successive cycles. Following incomplete conditioning (curve 1) the emission characteristics are typified by two regions of exponentially rising current (labelled a and c, respectively), separated by a plateau in emission current (region b). With continued conditioning however, distinct

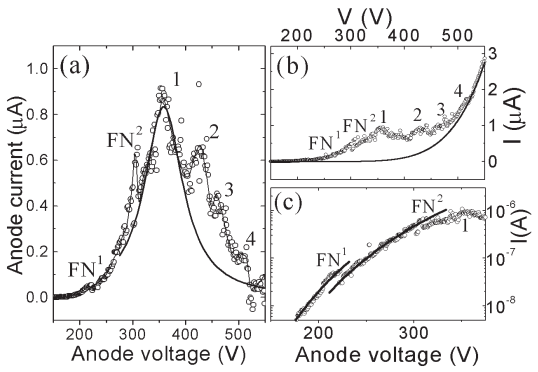

FIG. 4: (a) Field emission resonance region following subtraction of the background Fowler-Nordheim emission current as fitted to the *I–V* characteristics displayed in (b). (c) Semi–logarithmic plot of experimental data shown in (b). Solid lines indicate the best fits to current peaks FN^1 and FN^2.

current peaks develop within the current plateau region (see curves 2 and 3 of Fig. 3). The arrows indicate the positions of the five most prominent peaks. While the peak positions and relative intensities were found to be repeatable for each sample, a significant deviation in the number, position and intensity of peaks was observed between samples. While it is not possible to identify the individual nanostructure involved in electron emission, AFM images of the substrate surface, taken before and after field emission measurements, appear identical. Further, following exposure to air, it was found necessary to again condition the cathodes in order for the current peaks to develop, suggesting that conditioning is related to removal of adsorbates from the cathode surface.

The current peaks are also clearly observed when plotting the *I–V* characteristics on a Fowler-Nordheim plot [$\ln(I/V^2)$ versus $1/V$], as shown in the inset of Fig. 3 for curves 1 and 2. The Fowler–Nordheim plot also reveals highly linear behaviour at anode voltages > 550 V, suggesting electron emission through conventional (direct, non-resonant) Fowler–Nordheim tunnelling. The solid lines in Fig. 3, which display the Fowler–Nordheim relation fitted to the experimental data in this high voltage region, demonstrate excellent agreement between the model and observed emission current. Current peaks in the *I–V* characteristics of substrates containing multiple cathodes could be related to the activation and deactivation of additional emission sites.[23] However, the leading edge of each peak marked in the inset of Fig. 3 is found to be highly non-linear, suggesting conduction through a mechanism other than conventional Fowler–Nordheim tunnelling, in contrast to what would be expected from the activation of additional emission sites. This is in agreement with measurements performed using a phosphor–coated anode, which suggests electron emission from a *single emission site* over the range of anode voltage considered.

In order to study the current peaks in more detail, the background current fitted to the high–voltage Fowler–Nordheim tunnelling region was subtracted from the experimental data, as shown in Fig. 4(a). The corresponding *I–V* characteristics are displayed in Fig. 4(b). Four current peaks are observed (labelled 1–4) which supply an emission current 1.8 times greater than that predicted from conventional Fowler–Nordheim tunnelling. In addition to these symmetric current peaks, we find two highly asymmetric peaks, labelled FN^1 and FN^2 in Fig. 4. The presence of the asymmetric peaks becomes particularly apparent when the *I–V* characteristics of Fig. 4(b) are displayed on a semi-logarithmic plot, as shown in Fig. 4(c), where discontinuities aligned with peaks FN^1 and FN^2 are clearly observed. It is possible to match the experimentally observed field–emission resonance peaks to our theoretical results presented earlier. Fits to the line shape of peaks FN^1 and FN^2, shown by the solid lines in Fig. 4(c), yield pre-exponential factors of $V^{1.74}$ and $V^{1.704}$, respectively. This is very close to the theoretically expected power law $V^{5/3}$ predicted for resonant tunneling from the 3D substrate states. Furthermore, the Lorentzian line shape of resonance peaks labelled 1–4 [see Fig. 4(a)] is in good agreement to our theoretically predicted lineshape corresponding to resonant tunneling from the S–N accumulation layer. The excellent agreement between experiment and theory is a strong indication that resonant–tunneling transport as illustrated in Fig. 1 indeed occurs in our samples[24]. Additional numerical calculations based on previously described methods[10,11,12,13,14] and further modelling of sample electrostatics could yield the bound–state energies and their life–time broadening but these extended studies are beyond the focus of this work.

In conclusion, we have studied field emission from nanostructured surfaces that is strongly affected by resonant tunneling from both a 3D substrate and from 2D accumulation layers. Universal features in the current–voltage charateristics are derived theoretically and confirmed experimentally, and allow for identification of resonant–tunneling peaks with specific microscopic tunneling mechanisms. While the experimental part of this study considers resonant tunnelling from silicon nanostructure field–emission cathodes, the analytical expressions derived are quite generic and are applicable to a range of semiconductor structures used in the study of field–emission phenomena.

This work was performed under research contracts to the New Zealand Foundation for Research, Science and Technology (C05X0008, ‘Advanced industrial materials at the nanoscale’).

[1] R. H. Fowler and L. Nordheim, Proc. R. Soc. London **A119**, 173 (1928).
[2] L. Nordheim, Proc. R. Soc. London **A121**, 626 (1928).
[3] J. W. Gadzuk and E. W. Plummer, Rev. Mod. Phys. **45**, 487 (1973).
[4] M. E. Lin, R. P. Andres, and R. Reifenberger, Phys. Rev. Lett. **67**,

477 (1991).
[5] V. T. Binh, S. T. Purcell, N. Garcia, and J. Doglioni, Phys. Rev. Lett. **69**, 2527 (1992).
[6] H.-W. Fink, W. Stocker, and H. Schmid, Phys. Rev. Lett. **65**, 1204 (1990).
[7] V. G. Litovchenko, A. A. Evtukh, R. I. Marchenko, N. I. Klyui, and V. A. Seminovich, Appl. Surf. Sci. **111**, 213 (1997).
[8] V. Litovchenko, A. Evtukh, Yu. Kryuchenko, N. Goncharuk, O. Yilmazoglu, H. L. Hartnagel, and D. Pavlidis, J. Appl. Phys. **96**, 867 (2004).
[9] A. A. Dadykin, Yu. N. Kozyrev, and A. G. Naumovets, JETP Lett. **76**, 550 (2002); A. A. Dadykin, A. G. Naumovets, Yu. N. Kozyrev, M. Yu. Rubezhanska, P. M. Lytvyn, and Yu. M. Litvin, Prog. Surf. Sci. **74**, 305 (2003).
[10] V. G. Litovchenko and Yu. V Kryuchenko, J. Vac. Sci. Technol. B **11**, 362 (1993); Yu. V. Kryuchenko and V. G. Litovchenko, ibid. 14, 1934 (1996).
[11] Q.-A. Huang, J. Appl. Phys. **78**, 74 (1995).
[12] S. Vatannia, G. Gildenblat, and J. Schiano, J. Appl. Phys. **82**, 902 (1997).
[13] N. M. Goncharuk, Mat. Sci. Eng. **A353**, 36 (2003).
[14] R. Z. Wang, X. M. Ding, B. Wang, K. Xue, J. B. Xu, H. Yan, and X. Y. Hou, Phys. Rev. B **72**, 125310(R) (2005).
[15] T. T. Tsong, Surf. Sci. **81**, 28 (1979).
[16] R. Z. Wang, B. Wang, H. Wang, H. Zhou, A. P. Huang, M. K. Zhu, H. Yan, and X. H. Yan, Appl. Phys. Lett. **81**, 2782 (2002).
[17] J. H. Davies, *The Physics of Low-Dimensional Semiconductors* (Cambridge University Press, Cambridge, UK, 1998).
[18] To describe situations where the N–V quantum–well state is close to the top of the vaccum barrier, an improved version of the Fowler–Nordheim transmission functions needs to be used. See, e.g., K. L. Jensen, J. Vac. Sci. Technol. B **13**, 516 (1995).
[19] S. Johnson, A. Markwitz, M. Rudolphi, H. Baumann, S. P. Oei, K. B. K. Teo, and W. I. Milne, Appl. Phys. Lett. **85**, 3277 (2004).
[20] S. Johnson, A. Markwitz, M. Rudolphi, and H. Baumann, J. Appl. Phys. **96**, 605 (2004).
[21] S. Johnson, A. Markwitz, M. Rudolphi, H. Baumann, P. Y. Kuo, R. Blaikie, and A. Mücklich, J. Appl. Phys. **97**, 94301 (2005).
[22] G. L. Snider, I. -H. Tan, and E. L. Hu, J. Appl. Phys. **68**, 2849 (1990). This simulation program is available for download from `http://www.nd.edu/~gsnider` .
[23] A. A. G. Driskill-Smith, D. G. Hasko, and H. Ahmed, J. Vac. Sci. Technol. B **15**, 2773 (1997).
[24] The fact that our calculations were performed in the zero-temperature limit while measurements were taken at room temperature does not affect this conclusion. In particular, the predicted power law exhibited by the asymmetric peaks will hold as long as the IV curve shows the cut-off behaviour characteristic for resonant tunneling. However, tunneling from the 2D quantum-well states at the N–S interface should be strongly affected because, in our samples, their confinement energies are comparable to the room-temperature energy scale. This indeed explains the broad shape and small height of the symmetric peaks. Their Lorentzian form will be preserved, however, until such peaks are completely washed out.